ISSN 0031-918X, Physics of Metals and Metallography, 2020, Vol. 121, No. 7, pp. 675–682. © Pleiades Publishing, Ltd., 2020.
Russian Text © The Author(s), 2020, published in Fizika Metallov i Metallovedenie, 2020, Vol. 121, No. 7, pp. 742–749.

STRUCTURE, PHASE TRANSFORMATIONS, AND DIFFUSION

Structure and Texture Evolution of the Metastable Austenitic Steel during Cold Working

M. V. Odnobokova[a], *, A. N. Belyakov[b], I. N. Nugmanov[c], and R. O. Kaibyshev[b]

[a] *Institute for Physics of Advanced Materials, Ufa State Aviation Technical University, Ufa, 450008 Russia*
[b] *Belgorod State University, Belgorod, 308015 Russia*
[c] *Karimov' Tashkent State Technical University, Tashkent, 100123 Uzbekistan*
**e-mail: odnobokova_marina@mail.ru*

Received December 27, 2019; revised February 11, 2020; accepted March 10, 2020

Abstract—This work studies the structure and texture evolution in the 03Kh19N10 corrosion-resistant metastable austenitic steel (0.05C–18.2Cr–8.8Ni–1.65Mn–0.43Si–0.05P–0.04S wt %, and Fe for balance) during cold rolling, which results in twinning and martensitic transformation. The strain-induced martensite nucleates heterogeneously in the microshear bands and at their intersections. The fraction of strain-induced martensite increases with increasing true strain and approaches 80% at $e = 3$. The development of deformation twins, microshear bands, and martensitic crystallites results in the formation of a uniform nanocrystalline structure consisting of elongated γ/α' crystallites 100 nm in cross-section size after large deformation ($e = 2–3$). The austenite texture after cold rolling is characterized by the strong Brass ({110} ⟨112⟩) and Goss ({110}⟨001⟩) texture components, whereas the strain-induced martensite texture is characterized by strong texture component I* ({223}⟨110⟩) and an increased orientation density along γ fiber (⟨111⟩ ∥ ND). The orientation of the γ/α'-phase boundaries depends on the strain value.

Keywords: corrosion-resistant austenitic steel, cold rolling, deformation twinning, martensitic transformation, deformation texture

DOI: 10.1134/S0031918X20070066

INTRODUCTION

Developing the technologies for producing semifinished products from high-strength austenitic chromium–nickel steels [1–3] is an important task. These steels are widely used in various industries because of their corrosion properties. Heat treatment of austenitic chromium–nickel steels traditionally includes heating in the 1000–1100°C temperature range and fast cooling. This treatment fixes γ solid solution with homogeneously-distributed alloying elements and without $M_{23}C_6$ carbides, which provides the best corrosion properties [1, 4]. However, the austenitic chromium–nickel steels have a low strength after the traditional solid-solution treatment, which restricts their application as a structural material. The severe plastic deformation of austenitic steels increases their strength significantly both by producing ultrafine-grained (UFG) and nanocrystalline (NC) structures, as well as by producing strain-induced martensite [4–6]. The kinetics of the formation of these structures in materials with a fcc lattice is largely dependent on the stacking fault energy (SFE). Materials with low SFE (from 20 to 40 mJ/m^2) are characterized by a high rate of structural fragmentation due to deformation twinning [7–9]. Deformation twinning produces a high-density three-dimensional network of high-angle boundaries of deformation origin. This in turn improves the strength properties of the material due to both structural hardening by the Hall–Petch mechanism and dislocation hardening, since the maximum dislocation density increases by a factor of 5 or more as the crystalline size decreases from tens of microns to 20–40 nm [9, 10].

The corrosion-resistant austenitic chromium–nickel steel 03Kh19N10 (AISI 304L) [6] represents a material with a low stacking fault energy (~20 mJ/m^2). It should be noted that austenitic chromium–nickel steels are metastable at room temperature, since the temperature of the beginning of the $\gamma \rightarrow \alpha$ phase transformation lies in the 540–580°C temperature range. Room-temperature plastic deformation of metastable austenitic steels with this SFE is accompanied by martensitic transformation assisted by deformation twinning [1–3, 5, 7–9, 11–16]. The formation of strain-induced martensite leads to structure fragmentation due to the formation of interphase γ/α' boundaries [6, 11–14]. The formation of strain-induced martensite is known to obey the Kurdjumov–Sachs or Nishiyama–Wasserman crystallographic orientation relationships, at which interphase γ/α' boundaries with 45° angles are

formed [11, 15]. However, the stability of the γ/α' interphase during subsequent deformation has not been studied in sufficient detail [13]. The relationship between structure-forming mechanisms and texture evolution in metastable austenitic corrosion-resistant steels, the cold plastic deformation of which is accompanied by martensitic transformation, also remains unclear.

Depending on the mechanism of plastic deformation, there are two types of textures in fcc materials: copper texture ({112}⟨111⟩ and brass texture ({011}⟨211⟩) [6, 17–19]. The copper texture is observed in metals with high SFE, where the main mechanism of plastic deformation is sliding. The brass texture is typical of materials with low SFE, in which the main mechanism of plastic deformation is twinning. However, the effect of strain-induced martensite on the texture of metastable austenite has not been sufficiently studied. This work is aimed at studying the structural and textural evolution in the 03Kh19N10 austenitic corrosion-resistant metastable steel during severe plastic deformation by cold rolling.

EXPERIMENTAL

The object of the investigation was the 03Kh19N10 steel of the following chemical composition (wt %): 0.05C–18.2Cr–8.8Ni–1.65Mn–0.43Si–0.05P–0.04S, and Fe for balance. The preliminary thermomechanical treatment of the steel involved hot forging and annealing at 1100°C and subsequent water cooling. The plate rolling of the samples with an initial cross-section of 30 × 30 mm^2 was carried out at room temperature to obtain true strains $e \approx 0.5$, 1, 2, and 3. The structure was examined using a Jeol JEM-2100 transmission electron microscope (TEM) and a Nova Nanosem 450 scanning electron microscope (SEM) equipped with an electron back-scatter diffraction (EBSD) analyzer. The structural examination was conducted in the longitudinal section (perpendicular to the transverse direction of rolling) of the rolled samples. The size of crystallites (grains/subgrains) was calculated on TEM images by a linear-intercept method in the direction perpendicular to the rolling direction. Orientation distribution functions (ODF) were built using the EBSD maps with the aid of TSL OIM Analysis software. The volume fraction of martensite was estimated as an average value obtained by X-ray diffraction (XRD) analysis, and ferritoscope and EBSD methods.

RESULTS AND DISCUSSION

The preliminary treatment resulted in an initial microstructure with an average grain size of 21 μm [6, 15, 17]. Figure 1 shows the microstructure of the 03Kh19N10 austenitic corrosion-resistant steel after cold rolling. The cold rolling to a relatively small true strain $e = 0.5$ makes the initial austenitic grains elongated along the rolling direction and creates a low-angle subgrain boundary network inside the grains (Fig. 1a). The formation of the misoriented substructures can be explained by the difference in acting slip systems in various regions of the initial grains. Deformation twinning and martensitic $\gamma \rightarrow \alpha'$ transformation are also developed at the early stages of plastic deformation. The twinning causes further fragmentation of the austenitic grains due to the formation of coherent boundaries Σ3 with a misorientation angle of about 60°. The martensite transformation is responsible for the formation of a two-phase structure consisting of austenitic and martensitic grains (Fig. 1c). The fraction of the martensitic grains is about 0.2 (Fig. 2). Further cold rolling to a true strain of $e = 2$ provides an additional fragmentation and the formation of an ultrafine grain structure with mostly high-angle boundaries (Figs. 1b, 1d). The fraction of martensitic grains increases to 0.65 (see Fig. 2). The formation of the strain-induced martensite also stimulates structure fragmentation due to the formation of interphase γ/α' boundaries (Fig. 1d). The fraction of strain-induced martensite after rolling to $e = 3$ is close to the equilibrium fraction of the α ferrite that was calculated using the ThermoCalc program (see Fig. 2).

Figure 3 illustrates the fine structure of the 03Kh19N10 austenitic steel after cold rolling to various true strains. Figure 3a demonstrates a high density of deformation twins with the {111} twinning plane in the austenitic grains at the early stages of cold working. These twins look like thin plates about 50 nm thick. It should be noted that almost the entire grain volume is filled with a nanotwin structure (central part of Fig. 3a). Only one twin system acts in each grain. As a result, the initial austenitic grains 21 μm in size are fragmented into plates 50 nm thick, which are separated by coherent twin boundaries Σ3.

Since the secondary twinning does not develop in the 03Kh19N10 steel, the plastic deformation by the twinning mechanism is not possible. Plastic flow at $e = 1$ localizes to form microshear bands [7, 8]. The microshear bands are located at an angle of 30° to the rolling direction inside nanotwin stacks (Fig. 3b). Microshear bands and their intersections are mainly in the regions where the deformation martensite nucleates. Their formation increases the fraction of martensite at intermediate strain values. The plastic flow localization in the microshear bands induces further structural fragmentation. The microshear bands thus consist of slightly-elongated alternating γ/α' crystallites with a cross section of about 100 nm. Subsequent large deformation by cold rolling ($e = 2$, 3) makes the boundaries between the crystallites thinner, increases the misorientation between the boundaries of the shear bands, and changes (strongly deviates from 60.4°) the misorientation of special boundaries (that become incoherent), as indicated by ring electron diffraction patterns (Figs. 3c, 3d). Due to the formation of microshear bands and deformation martensitic

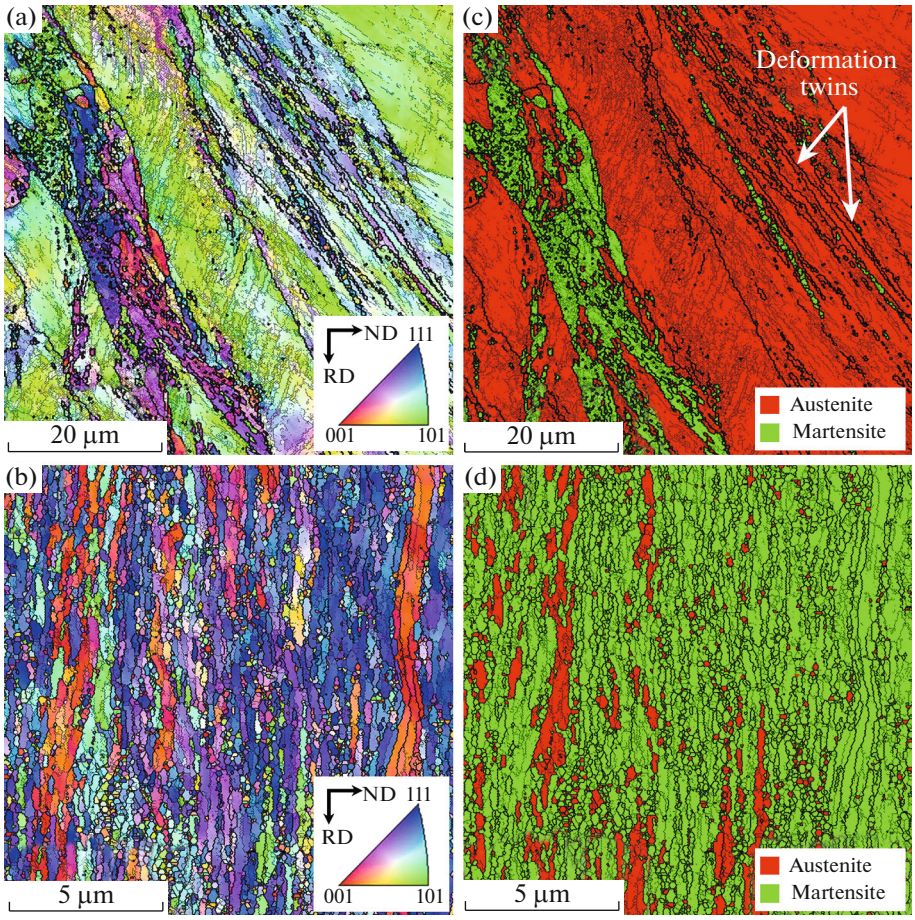

Fig. 1. (a), (b) Microstructure and (c), (d) phase composition of the 03Kh19N10 austenitic corrosion-resistant steel after cold rolling at (a), (c) $e = 0.5$ and (b), (d) 2. The crystallographic direction along the normal (ND) to the rolling plane is indicated by the color in (a) and (b) images.

crystallites, there is a transition from a two-dimensional twin nanostructure to a three-dimensional mixed structure. The cold rolling to $e = 3$ forms a structure that consists of austenitic and martensitic nanocrystallites with a transverse size of about 80 nm. The nanocrystallites are strongly elongated along the rolling direction.

Figure 4 shows the distribution of γ/α' interphase grain boundaries misorientation after the cold rolling of the 03Kh19N10 steel. The distribution of γ/α'-interphase grain boundaries misorientation exhibits one peak that corresponds to angles of about 45°. This peak is associated with the strain-induced martensite transformation that occurs by the shear mechanism, since the orientation relations between austenite and martensite in corrosion-resistant steels are close to those of Kurdyumov–Sachs and Nishiyama–Wasserman, which correspond to misorientation between γ and α phases at 42.9° and 46°, respectively [11, 15]. At relatively small true strains $e = 0.5$ and 1, the peak corresponding to the angles of about 45° is acute (Figs. 4a, 4b) due to the formation of new martensitic

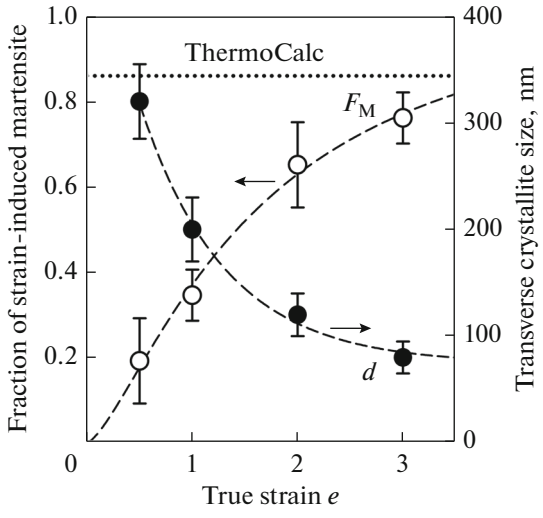

Fig. 2. Effect of true strain e on fraction of strain-induced martensite F_M and transverse size of crystallites d in the 03Kh19N10 corrosion-resistant austenitic steel.

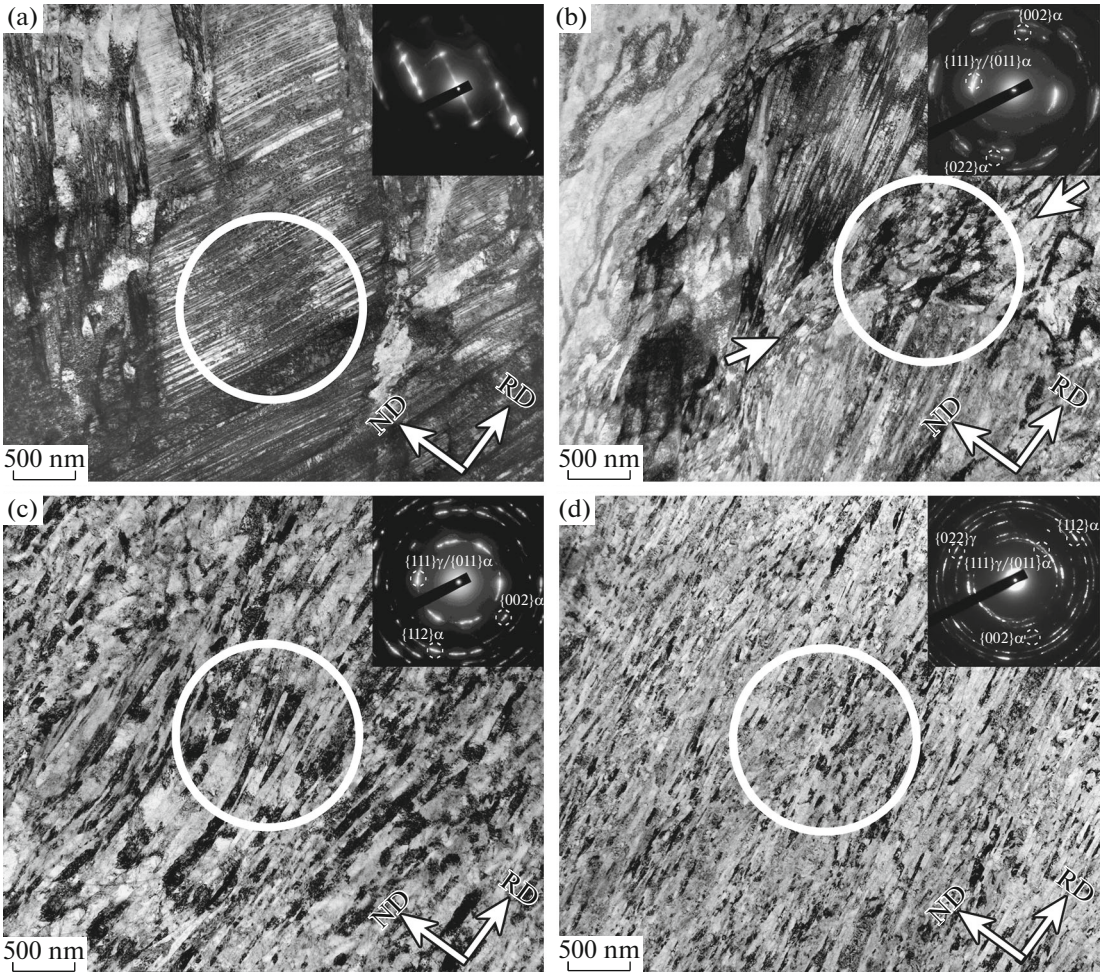

Fig. 3. Fine structure of the 03Kh19N10 austenitic corrosion-resistant steel after cold rolling at true strains *e*: (a) 0.5, (b) 1, (c) 2, and (d) 3. Regions where the electron diffraction patterns were taken are circled.

grains. However, the maximum fraction of interphase boundaries corresponds to an angle of 46°, i.e., the Nishiyama–Wasserman orientation relationship is fulfilled mainly between austenitic and martensite grains [11, 15]. Subsequent cold rolling at $e = 2$ and 3 results in the formation of both new martensitic crystallites, since the fraction of deformation martensitic is gradually increasing over the entire true strain range, and the reorientation of previously formed γ/α' interphase boundaries. The peak corresponding to ~45° (see Figs. 4c, 4d) is blurred towards the interphase boundaries with a misorientation of about 35°. Consequently, the deformation process reorients the γ/α' interphase boundaries, resulting in two peaks at angles of about 35° and 45°.

Figure 5a is a schematic representation of orientation distribution functions (ODFs) of the main texture components for austenite and martensite. Their Euler coordinates are given in Table 1. Figure 5b shows the ODFs for the 3Kh19N10 austenitic steel after cold rolling to various true strains. The texture of the austenite after cold rolling is characterized by the formation of a higher orientation density along the ζ fiber ($\langle 110 \rangle \parallel$ ND) and γ fiber ($\langle 111 \rangle \parallel$ ND). The ζ fiber is characterized by two pronounced maximal intensities near the Brass ({110}112) and Goss ({110}001) texture components, which are typical of rolled fcc materials with low or medium stacking fault energies that are usually deformed by twinning and with shear band formation. Thus, the ζ fiber appears in the austenite texture after relatively small deformation and becomes stronger with increasing true strain. It is worth noting that the fraction of the Brass texture component prevails over the fraction of the Goss texture component in the entire strain range under consideration [6]. The formation of the γ fiber and maximum intensities, which correspond to the E ($\{111\}\langle 110 \rangle$) and F ($\{111\}\langle 112 \rangle$) texture components, is associated with the formation of ultrafine grains in the shear bands. The γ fiber forms in the true strain range from 1 to 2. However, its formation slows down with increasing true strain, when the crystallites are reoriented within pre-

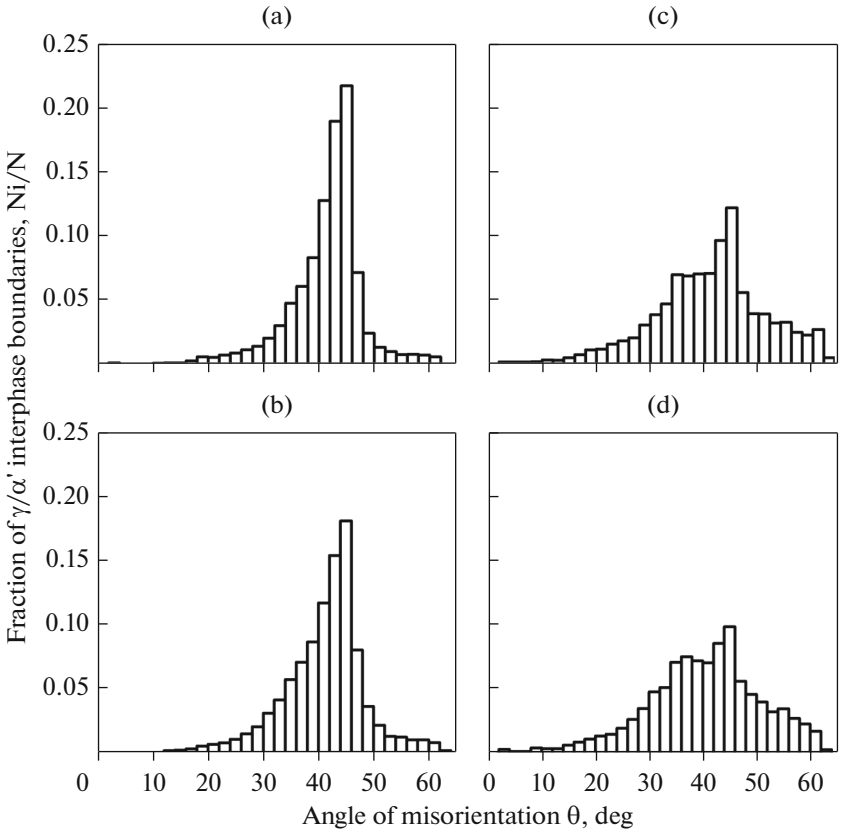

Fig. 4. Distribution of γ/α' interphase grain boundary misorientations in the 03Kh19N10 austenitic corrosion-resistant steel after cold rolling at true strains *e*: (a) 0.5, (b) 1, (c) 2, and (d) 3.

viously formed shear bands. In addition, the E and F texture components become less pronounced due to the martensite transformation process, which develops easily in microshear bands, and therefore decreases the fraction of orientations associated with shear bands in austenite.

After cold rolling the texture of the strain-induced martensite is characterized by the development of η fiber (⟨001⟩ ∥ ND) and γ fiber (⟨111⟩ ∥ ND). The η fiber with maximum intensities near the H({001} ⟨110⟩) texture component becomes more pronounced at $e = 2$ and is remained the same at $e = 3$. The γ fiber exhibits a high orientation density near the F ({111} ⟨112⟩) texture component at relatively small true strain $e = 1$. The formation of the F texture component in the martensite texture at the first stage of plastic deformation

Table 1. Textural components that are typical of austenite and martensite

Component, symbol	{*hkl*}⟨*uvw*⟩	Euler angles		
		φ_1	Φ	φ_2
Cube (C)	{001}⟨100⟩	45	0	45
Rotated cube (H)	{001}⟨110⟩	0/90	0	45
E	{111}⟨110⟩	0/60	55	45
F	{111}⟨112⟩	30/90	55	45
I*	{223}⟨110⟩	0	43	45
Goss (G)	{110}⟨001⟩	90	90	45
Rotated Goss (RtG)	{110}⟨110⟩	0	90	45
Brass (B)	{110}⟨112⟩	55	90	45
A	{110}⟨111⟩	35	90	45
Copper (Cu)	{112}⟨111⟩	90	35	45

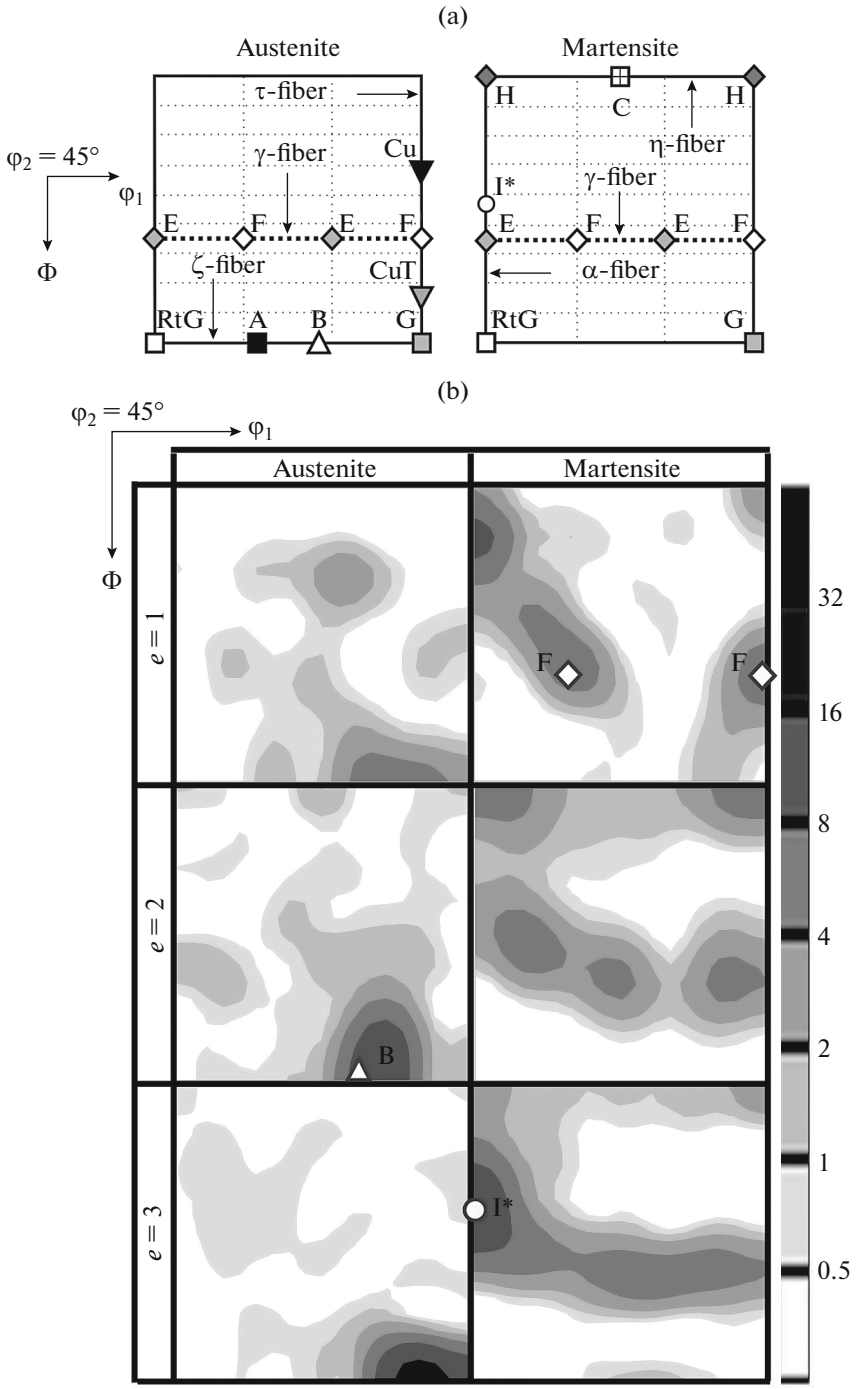

Fig. 5. (a) Schematic representation of the ODFs of the main texture components for austenite and martensite. (b) ODFs of the 03Kh19N10 austenitic corrosion-resistant steel after cold rolling at various true strains.

is associated with the $\gamma \rightarrow \alpha'$ shear phase transformation according to the Kurdyumov–Sachs and Nishiyama–Wasserman orientation relations, as a result of the transformation of the austenite with the Brass texture component (Fig. 6) [6]. An increase in the true strain leads to an alignment of the orientation density along the entire γ fiber. It should be noted that the strain-induced martensite after large true strain $e = 3$ is characterized by a strong texture component I* ({223} ⟨110⟩) that is usually attributed to the base slip system, namely {110} ⟨111⟩ in bcc metals. The I* texture component is more stable than the F texture component, which additionally confirms the reorientation of the γ/α' interphase boundaries (resulting from the

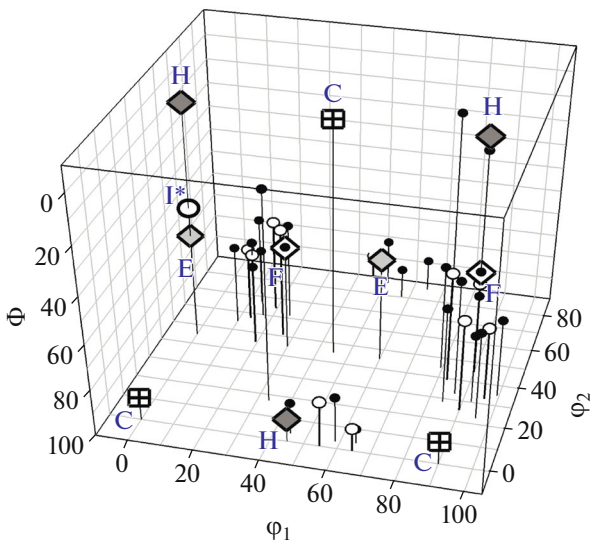

Fig. 6. Martensite orientation resulted from the austenite transformation at the {110}⟨112⟩ Brass component according to Kurdyumov–Sachs and Nishiyama–Wasserman orientation relationships.

shear martensite transformation) during the deformation process. The angles between martensite and austenite, between the I* and Brass and between I* and Goss orientations are 31° and 45°, respectively. Thus, there are two particular peaks in the misorientation distribution for interphase boundaries due to the formation of the I* texture component.

CONCLUSIONS

The cold rolling of the 03Kh19N10 austenitic corrosion-resistant steel is accompanied by deformation twinning and martensite formation, and therefore, rapid microstructure fragmentation. Microshear banding at intermediate true strains facilitates the transformation of the strain-induced martensite and, hence, increases its volume fraction. The martensitic transformation occurs according to the Kurdjumov–Sachs and Nishiyama–Wasserman crystallographic orientation relationships. This fact is supported by the formation of γ/α' interphase boundaries with an angle of 45°. A large fraction of γ/α' interphase boundaries have a misorientation of 46°; i.e., the strain-induced martensite mainly forms according to the Nishiyama–Wasserman orientation relationship. As the true deformation increases, the austenitic and martensite crystallites reorient. As a result, the γ/α' interphase boundaries tend to a more stable orientation with a 35° misorientation. The nanocrystalline structure that comprises severely elongated austenitic and martensitic grains/subgrains with a cross-section size of about 80 nm, is formed during cold rolling at $e = 3$. The austenite texture evolution during the cold rolling is characterized by an increase in Brass ({110}⟨112⟩) and Goss ({110}⟨001⟩) components that form ζ fiber (⟨110⟩ ∥ ND). The martensite texture at the intermediate true strains is described by F ({111}⟨112⟩) strong texture component. The γ → α' phase transformation that is described by the Kurdyumov–Sachs and Nishiyama–Wasserman orientation relationships, is responsible for the appearance of the F component. The I* ({223}⟨110⟩) component tends to increase with increasing the true strain. This fact points to its more stable orientation and, as a consequence, to the reorientation of γ/α' interphase boundaries formed by the martensite-transformation shear mechanism.

FUNDING

The reported study was funded by RFBR, project number 19-38-60047.

REFERENCES

1. K. H. Lo, C. H. Shek, and J. Lai, "Recent developments in stainless steels," Mater. Sci. Eng., R **65**, 39–104 (2009).
2. A. V. Makarov, P. A. Skorynina, E. G. Volkova, and A. L. Osintseva, "Effect of heating on the structure, phase composition, and micromechanical properties of the metastable austenitic steel strengthened by nanostructuring frictional treatment," Phys. Met. Metallogr. **119**, 1196–1203 (2018).
3. A. V. Makarov and L. G. Korshunov, "Metallophysical foundations of nanostructuring frictional treatment of steels," Phys. Met. Metallogr. **120**, 303–311 (2019).
4. V. V. Sagaradze and A. I. Uvarov, *Strengthening of Austenitic Steels* (Nauka, Moscow, 1989) [in Russian].
5. V. V. Sagaradze and A. I. Uvarov, *Strengthening and Properties of Austenitic Steels* (RIO UrO RAN, Ekaterinburg, 2013) [in Russian].
6. M. Odnobokova, A. Belyakov, and R. Kaibyshev, "Grain refinement and strengthening of austenitic stainless steels during large strain cold rolling," Philos. Mag. **99**, 531–556 (2019).
7. T. Sakai, A. Belyakov, R. Kaibyshev, H. Miura, and J. J. Jonas, "Dynamic and post-dynamic recrystallization under hot, cold and severe plastic deformation conditions," Prog. Mater. Sci. **60**,130–207 (2014).
8. P. S. Kusakin and R. O. Kaibyshev, "High-Mn twinning-induced plasticity steels: Microstructure and mechanical properties," Rev. Adv. Mater. Sci. **44**, 326–360 (2016).
9. Z. Yanushkevich, A. Belyakov, C. Haase, D. A. Molodov, and R. Kaibyshev, "Structural/textural changes and strengthening of an advanced high-Mn steel subjected to cold rolling," Mater. Sci. Eng., A **651**, 763–773 (2016).
10. M. V. Karavaeva, M. M. Abramova, N. A. Enikeev, G. I. Raab, and R. Z. Valiev, "Superior strength of austenitic steel produced by combined processing, includ-

ing equal-channel angular pressing and rolling," Metals **6** (12), 310 (2016).

11. N. Nakada, H. Ito, Y. Matsuoka, T. Tsuchiyama, and S. Takaki, "Deformation-induced martensitic transformation behavior in cold-rolled and cold-drawn type 316 stainless steels," Acta Mater. **58**, 895–903 (2010).
12. I. I. Kositsyna and V. V. Sagaradze, "Phase transformations and mechanical properties of stainless steel in the nanostructural state," Bull. Russ. Acad. Sci.: Phys. **71**, 285–288 (2007).
13. I. Yu. Litovchenko, A. N. Tyumentsev, N. V. Shevchenko, and A. V. Korznikov, "Evolution of structural and phase states at large plastic deformations of an austenitic steel 17Cr–14Ni–2Mo," Phys. Met. Metallogr. **112**,412–423 (2011).
14. A. N. Tyumentsev and I. Y. Litovchenko, "Models of dislocation formation and mechanical twinning by local reversible martensitic transformations in FCC nanocrystals," Adv. Mater. Res. **1013**, 234–241 (2014).
15. M. Odnobokova, A. Belyakov, and R. Kaibyshev, "Development of nanocrystalline 304L stainless steel by large strain cold working," Metals **5**, 656–668 (2015).
16. V. Kraposhin, I. Jakovleva, L. Karkina, G. Nuzhny, T. Zubkova, and A. Talis, "Microtwinning as a common mechanism for the martensitic and pearlitic transformations," J. Alloys Compd. **577**, 30–36 (2013).
17. M. V. Odnobokova and A. N. Belyakov, "Effect of cold rolling and subsequent annealing on the microstructure and the microtexture of austenitic corrosion-resistant steels," Russ. Metall. (Metally) **2019**, 315–325 (2019).
18. S. S. Gorelik, S. V. Dobatkin, and L. M. Kaputkina, *Recrystallization of Metals and Alloys* (MISiS, Moscow, 2005) [in Russian].
19. T. Leffers and R. K. Ray, "The brass-type texture and its deviation from the copper-type texture," Prog. Mater. Sci. **54**, 351–396 (2009).

Translated by T. Gapontseva